

A Three Parsec-Scale Jet-Driven Outflow from Sgr A*

F. Yusef-Zadeh¹, R. Arendt², H. Bushouse³, W. Cotton⁴, D. Haggard¹, M. W. Pound⁵, D. A. Roberts¹, M. Royster¹ and M. Wardle⁶

¹*Department of Physics and Astronomy and Center for Interdisciplinary Research in Astronomy, Northwestern University, Evanston, IL 60208*

²*CREST/UMBC/NASA GSFC, Code 665, Greenbelt, MD 20771*

³*Space Telescope Science Institute, 3700 San Martin Drive, Baltimore, MD 21218*

⁴*National Radio Astronomy Observatory, Charlottesville, VA 22903*

⁵*University of Maryland, Department of Astronomy, MD 20742*

⁶*Dept of Physics and Astronomy, Macquarie University, Sydney NSW 2109, Australia*

ABSTRACT

The compact radio source Sgr A* is coincident with a $4 \times 10^6 M_\odot$ black hole at the dynamical center of the Galaxy and is surrounded by dense orbiting ionized and molecular gas. We present high resolution radio continuum images of the central 3' and report a faint continuous linear structure centered on Sgr A* with a PA $\sim 60^\circ$. The extension of this feature appears to be terminated symmetrically by two linearly polarized structures at 8.4 GHz, $\sim 75''$ from Sgr A*. A number of weak blobs of radio emission with X-ray counterparts are detected along the axis of the linear structure. The linear structure is best characterized by a mildly relativistic jet from Sgr A* with an outflow rate $10^{-6} M_\odot \text{ yr}^{-1}$. The near and far-sides of the jet are interacting with orbiting ionized and molecular gas over the last 1–3 hundred years and are responsible for a 2'' hole, the “minicavity”, characterized by disturbed kinematics, enhanced FeII/III line emission, and diffuse X-ray gas. The estimated kinetic luminosity of the outflow is $\sim 1.2 \times 10^{41} \text{ erg s}^{-1}$, so the interaction with the bar may be responsible for the Galactic center X-ray flash inferred to be responsible for much of the fluorescent Fe K α line emission from the inner 100pc of the Galaxy.

Subject headings: accretion, accretion disks — black hole physics — Galaxy: center

1. Introduction and Observations

Stellar orbits within $1''$ of the compact radio source Sgr A* at the dynamical center of the Galaxy are compelling evidence for a $4 \times 10^6 M_\odot$ black hole (Ghez et al. 2008; Gillessen et al. 2009; Reid and Brunthaler 2004). This compact source is ~ 100 times closer to us than the next nearest example of a supermassive black hole and presents an unparalleled opportunity to study the processes by which gas is captured, accreted and ejected from black holes. Observations of Sgr A* thus far have revealed no hard evidence for a small-scale jet or an accretion disk, and thus the relative ratio of the accretion and outflow rates is unknown. We have recently reanalyzed archival radio and X-ray continuum and molecular line data that were taken with the Very Large Array (VLA) of the National Radio Astronomy Observatory¹ (NRAO), *Chandra* X-ray Observatory, and the Combined Array for Research in Millimeter-wave Astronomy (CARMA) observations of the inner few pc of Sgr A* to search for interaction sites of a jet with the surrounding material near Sgr A*.

The inner pc of the Galactic center contains diffuse ionized gas, e.g., Sgr A West which orbits Sgr A* (Lacy et al. 1980; Ferriere et al. 2012). Sgr A West with its three-arm mini-spiral appearance, consists of the W arm or arc, which is coupled to the Circumnuclear Molecular Ring (CMR), and the E and N arms of ionized gas. With a closest projected distance of ~ 0.1 pc, Sgr A West shows a bright bar of ionized gas, within which a hole or the “minicavity” with a diameter of $2''$ is noted. A chain of circular-shaped radio blob structures links Sgr A* to the “minicavity” by a ridge of emission at 8.4 GHz (Yusef-Zadeh, Morris & Ekers 1990; Wardle & Yusef-Zadeh 1992). The minicavity shows enhanced FeIII line emission, a high electron temperature and is kinematically disturbed, having radial velocities ranging between -150 and -290 km s⁻¹ at its edge and a highly blue shifted velocity ~ -340 km s⁻¹ in the interior (Eckart et al. 1990; Lacy et al. 1991; Lutz et al. 1993; Roberts et al. 1996; Zhao et al. 2009). The kinematic structure may be explained by a shock due to a hot bubble expanding at a velocity of 180 km s⁻¹ (Lutz et al. 1993). Here, we present a faint, highly collimated linear structure observed at radio wavelengths which is associated with the ridge of emission linking Sgr A* to the minicavity. We argue that this is a synchrotron emitting jet from Sgr A* and the blobs are sites of dynamical interaction with orbiting gas.

The radio data presented here were taken at 4.85 (6 cm), 8.4 (3.6 cm), 15 (2 cm), 22 (1.3 cm) and 42 (7mm) GHz using multiple configurations of the VLA. The radio data are self-calibrated in phase to remove atmospheric phase errors as well as properly correcting the time variability of Sgr A*, by fitting a point source model in the visibility plane. The X-ray data derives $\sim 1.4 \times 10^6$ seconds of archival *Chandra* ACIS-I observations taken between 2000-10-26 and 2011-03-31 which were recalibrated and combined using CIAO 4.4 (CALDB 4.4.8; Fruscione et al. 2006). The merged 0.5–10 keV image has a resolution of $0.492''$ and is normalized at 2.3 keV. The SiO data were obtained with CARMA during the 2009 and 2010 observing seasons in the D and C array configurations. The array consisted of six 10.4m antennas and nine 6.1m antennas and the maps were made on a 127-point hexagonal

¹The National Radio Astronomy Observatory is a facility of the National Science Foundation, operated under a cooperative agreement by Associated Universities, Inc.

mosaic, Nyquist-sampling the 10.4m antenna primary beam. The spatial resolution and spectral resolutions of the final maps are $8.0'' \times 4.1''$ and 6.74 km s^{-1} , respectively, and the 1σ rms noise is 90 mJy/beam .

Figure 1a,b show grayscale 22 and 15 GHz, high dynamic range ($\sim 10^4$), images of the inner $30''$ of Sgr A*. We note a new linear feature in both images running diagonally crossing the bright N and W arms of the mini-spiral, along which several blobs (b, c, d, h1 and h2) are detected. These images best reveal the continuity of the linear feature along a position angle of $\sim 60^\circ$ (E of N) extending symmetrically with respect to Sgr A*. The linear feature to the SW is thicker and brighter than that of the NE by a factor of 1.5-2, respectively. The southern tip of this continuous $30''$ feature appears to cross the W arm and becomes brighter from 0.2 mJy to about 1 mJy at 22 GHz. A bow-shock-like structure is detected at the position where the linear feature crosses the W arm near $\alpha, \delta(\text{J2000}) 17^{\text{h}} 45^{\text{m}} 38^{\text{s}}.9, -29^\circ 00' 38''$. On the NE of Sgr A*, blob h1 is extended in the direction of the linear feature. Figure 1c shows a closeup view of the linear feature at 8.4 GHz within $8'' \times 6''$ of Sgr A* where a ridge of emission linking blob ϵ to Sgr A*. The ridge of emission is also seen as a linear feature at 42 GHz in Figure 1d. We note that the weak linear feature at 42 GHz extends for $2''$ pointing toward the brightest segment of the western rim of the minicavity where several compact continuum sources are detected. The morphology of the emission suggests that the linear feature is impacting the mini-cavity. A “dark radio cloud” labeled on Figure 1d is interpreted as an embedded molecular cloud associated with the mini-cavity, as discussed elsewhere, showing a deficiency of radio continuum emission.

Unlike total intensity, the polarized emission from the region near Sgr A* is not confusion-limited. Figure 2a shows the detection of linearly polarized contours of emission superimposed on the corresponding total intensity image at 8.4 GHz. The polarized features SgrA-P1-P4 are placed to NE and SW of Sgr A*. The brightest polarized features are aligned along the continuous linear feature, as seen in high resolution images (cf., Fig. 1), with the total projected extent of $\sim 150''$ ($\sim 6 \text{ pc}$). Figure 2b shows high resolution polarized image of the emission at 8.4 GHz. New polarized sources SgrA-P1 ($17^{\text{h}} 45^{\text{m}} 43^{\text{s}}.6, -28^\circ 59' 22''$), P2 ($17^{\text{h}} 45^{\text{m}} 43^{\text{s}}.3, -29^\circ 00' 12''$), P3 ($17^{\text{h}} 45^{\text{m}} 43^{\text{s}}.6, -29^\circ 00' 08''$) located $\sim 75'', 45''$ and $60''$ NE of Sgr A* and P4 ($17^{\text{h}} 45^{\text{m}} 34^{\text{s}}.8, -29^\circ 01' 09''$) lying $75''$ SE of Sgr A*. The brightest polarized feature P1 shows filamentary structure, extending for $\sim 25''$. The lower limit to fractional polarization of P1 to P4 at 8.4 GHz are 15%, 5%, 1-2% and 8%, respectively. A common characteristic of polarized features SgrA-P1 to P4 is that they are azimuthally extended in the direction perpendicular to the orientation of the linear feature. In addition to the P1-P4 polarized sources, we also notice a weak linearly polarized filament with an extent of $< 1'$ to the south of Sgr A*, labeled P5 in Figure 2b. The extension of the linear feature to the NE and SW crosses the concentration of molecular gas associated with the CMR. To examine the possibility that polarized features are physically associated with the molecular ring, Figure 2c shows the clumpy distribution of SiO (2-1) emission. The linearly polarized features SgrA-P1 to P4 appear to be spatially correlated with SiO emission, which is known to be an excellent indicator of shocked molecular gas. Polarized features, in particular, appear to be located at the edge of molecular clumps. P4 appears to be associated with an isolated molecular clump traced by HCN line emission (Christopher et al. 2005).

The spectrum of the HCN clump at the position of P4 shows two velocity components at -43 and -120 km s $^{-1}$.

Although there is no polarized emission detected from Sgr A* at a level of less than 0.1%, we notice weak polarized emission at a level of 50-100 μ Jy within the inner few arcseconds of Sgr A*. Figure 2d shows contours of 8.4 GHz emission superimposed on diffuse polarized emission with a fractional polarization $\sim 0.5\%$ outside Sgr A*. The diffuse polarized emission is elongated along the axis that links P1 and P4 and the overall electric vector distribution of weak polarized emission outside Sgr A* runs perpendicular to the axis of the elongation. Using the upper limit flux density of ~ 1 mJy per $0.35'' \times 0.2''$ beam, the equipartition magnetic fields are 1.6, 1.9 and 5.9 mG for proton to electron ratio of 0, 1 and 100, respectively.

Figure 3a shows a 8.4 GHz image of the inner $\sim 45'' \times 30''$ of Sgr A*. The bright central source coincides with Sgr A* surrounded by the three arms of the mini-spiral and the bar of ionized gas within which the “minicavity” lies. SgrA-a1, a2, b, c, d and e, are identified to the west of Sgr A* crossing the ionized flow associated with the W arm. The ϵ blob, which was originally detected at 15 GHz (Yusef-Zadeh, Morris and Ekers 1990), is the brightest of all the blobs and lies about $1''$ to the west of Sgr A*, followed by two blobs a1 and a2 lying at the western boundary of the minicavity. The SgrA-blobs f, g and h are detected to the east of Sgr A* crossing the N arm of Sgr A West. The peak flux density of the blobs a1 and a2 range between 0.1 to 0.3 mJy beam $^{-1}$. Figure 3b shows a 22 GHz image displaying diffuse emission lying between the W arm and the minicavity. A weak circular-shaped feature surrounding blob a1 and a2 with an X-ray counterpart (c.f. G359.942-0.045 in Fig. 5) is detected with a diameter of $0.33''$. The integrated flux density of the circular-shaped feature which lies immediately adjacent to the minicavity, is ~ 29 mJy (cf, Figs. 4a and 5a).

Figure 4a,b show a 22 GHz VLA and 2-4 keV Chandra image of the inner $25'' \times 18''$ of Sgr A*, respectively. One of the new radio features that is revealed in Figure 4a is a $\sim 2''$ tear-drop shaped bubble roughly centered around Sgr A*. This bubble is open on the northern side with a morphology that resembles the shape of the minicavity. Detailed analysis of Chandra data suggests that X-ray emission from Sgr A* is spatially extended (Baganoff et al. 2003). However, the coincidence of the extended X-ray emission from Sgr A* with the tear-drop suggests that the extended X-ray component is likely produced by the synchrotron jet from Sgr A* or shocked winds by mass-losing stars orbiting Sgr A*, as the ram pressure of the winds pushing the ionized bar away and create a tear-drop cavity .

There are four diffuse and compact X-ray sources that have previously been identified, Sgr A*, IRS 13, G359.945-0.044 (a PWN candidate) and G359.943-0.047 (Baganoff et al. 2003; Wang et al. 2006; Munro et al. 2008, 2009), as labeled in Figure 4a,b. There are two faint extended X-ray sources symmetrically placed with respect to Sgr A*. One is an elongated loop-like structure (labeled NE plume in Figure 4) to the NE of Sgr A* with an extension of $8'' \times 2''$. The SW plume is more difficult to discern because of the bright source IRS 13 and the transient source G359.943-0.047. However, the X-ray source G359.942-0.045, which has a radio counterpart (blob b in Figures 1 and 4), appears to be a part of the SW plume. The two extended plume-like features lie along the axis in which the continuous linear structure

is detected at radio wavelengths. There are also weak X-ray features noted in the immediate vicinity of the N arm, G359.947-0.047 in Figure 4b, along the same axis as the linear radio feature. The X-ray emission adjacent to the N arm provides a strong evidence that an energetic event is responsible for X-ray emission.

Our high resolution radio and X-ray continuum images show new structural details within 5 pc of Sgr A*. We detect a chain of faint blobs which are distributed along a continuous linear feature. The linear feature continues beyond the ionized arms of Sgr A West, extending to about $75''$ (3pc) away from Sgr A* before it is terminated by extended linearly polarized features. The orientation of the collimated feature is consistent with proper motion and cometary morphology of dust features as well as the bow shock structure of FeII line emission leading to the idea of an outflow from young massive stars or from Sgr A* (Lutz et al. 1993; Muzic et al. 2007). The collimated feature could be produced by the winds of massive young stars associated with the clockwise rotating stellar disk (Paumard et al. 2006). However, it is not clear how to collimate the outflowing winds. Numerical simulations of wind-wind collisions incorporating the dynamics of stars in the central cluster do not show any evidence of collimated structure (Cuadra et al. 2008). Thus, it is more likely that Sgr A* itself is responsible for the origin of the collimated feature and the acceleration of particles to high energies.

We account for the origin of the new features in terms of a mildly relativistic jet symmetrically emanating from Sgr A*. The jet interacts with the orbiting gas, forms the structure of the minicavity, compresses and shocks the gas producing X-ray and radio emitting blobs of emission. The brightest polarized features are symmetrically placed at a projected distance of $\sim 3\text{pc}$ from Sgr A* and are consistent with the jet picture. The lack of polarized emission at 8.4 GHz from the inner pc is due to depolarization by dense ionized gas.

The near and far side components of the symmetrical jet run into the ionized bar and the N arm which are assumed to be located in the front and back side of Sgr A*, respectively. In this picture, the ionized bar and the N arm are two independent ionized features orbiting Sgr A* (Zhao et al. 2009). The ram pressure of the near-side component of the jet disturbs the ionized bar and produces the high negative velocity at the western edge of the minicavity. The change in the velocity of the gas is about 100 km s^{-1} between the E and W boundaries of the minicavity. The blue-shifted gas associated with the bar gets more blue-shifted at the interaction site. Similarly, the far side component of the jet punches through the N arm and causes a sinusoidal pattern along the clockwise motion of the N arm. If we assume that the jet is mildly relativistic, it can punch through the 10^5 cm^{-3} gas of the bar. On the other hand if the jet missed the bar originally and then the bar is currently sweeping around it, the jet can survive deflection and the interaction might create the minicavity.

The mass outflow rate in the jet should be somewhat less than the accretion rate onto Sgr A*, which is estimated to be a few times $10^{-5}\text{ }M_{\odot}\text{ yr}^{-1}$ (e.g. Cuadra et al. 2008). We adopt a nominal mass outflow rate of $10^{-6}\text{ }M_{\odot}\text{ yr}^{-1}$, a Lorentz factor $\gamma \sim 3$, and a cross-section equivalent to a diameter of $1''$. Then the momentum transfer rate $\dot{M}\gamma v = 0.3\text{ }\gamma\text{ }M_{\odot}\text{ yr}^{-1}\text{ km s}^{-1}$, sufficient to drive a $270\gamma^{0.5}\text{ km s}^{-1}$ shock into the 10^5 cm^{-3} molecular gas associated with the bar. The interaction of this gas with the jet may then be responsible for the minicavity,

which exhibits a velocity disturbance of $100\text{--}200\text{ km s}^{-1}$ (Roberts et al. 1996), suggesting an age of approximately 100–300 years for this interaction. The gas would be shock-heated to about 3 million K, with a cooling time of only a few years, and the X-ray luminosity of the cooling gas is of order the kinetic luminosity of the jet. If the interaction only lasted for 1–2 decades, it would have produced the X-ray flash thought to be responsible for much of the fluorescent 6.4 keV Fe $K\alpha$ line emission within 100 pc of the Sgr A* (Sunyaev & Churazov 1998; Koyama et al. 2009).

The jet continues crossing the W and N arms and eventually interacts with the molecular ring where linearly polarized emission is detected. The wider thickness and higher surface brightness of the jet to the SW, compared to that of NE are consistent with a higher density of material distributed in the dense ionized bar. The jet drives shocks into gas clouds producing blobs of X-ray emitting gas, shocked molecular H_2 and SiO emission, enhancing the iron abundance in the gas phase, generating a low dust to gas ratio in the minicavity and disturbing the kinematics of orbiting ionized gas.

The collimation of the outflowing material from Sgr A* along a jet axis is generally considered to be due to an accretion disk. The axis of the jet outflow from Sgr A* is estimated to be 60° . This position angle of large-scale jet differs by $30^\circ - 60^\circ$ from the constraints placed by VLBA measurements (Markoff, Bower and Falcke 2007). Notably, the orientation of the jet, indicated by dashed line in schematic diagrams of Figure 4c,d runs perpendicular to the principal axis of the clockwise stellar disk (Paumard et al. 2006). This alignment may be a coincidence or possibly due to the accretion processes that still continue in forming young low-mass stars. If so, Sgr A* is retaining the memory of in-situ star formation activity in its vicinity. Almost all models of the steady component of the emission from Sgr A* predict an accretion disk, a jet and/or an outflow. Present observations support jet models for Sgr A* (e.g., Falcke and Markoff 2000; Das et al. 2009; Becker et al. 2011).

In summary, we have presented evidence for a faint pc scale linear feature arising from Sgr A* that interacts with ionized and molecular material orbiting Sgr A*. An important implication of a jet/outflow is that a disk is needed to collimate the outflowing materials. Given that the VLA is a linear array, deconvolution errors may result linear structures along the symmetric beam pattern with the beam being strongest in the NS direction for southern sources. Our images do not show any evidence of symmetric “cross” pattern. However, future observations with non-linear arrays, such as ALMA, should confirm the reality of polarized jet associated with Sgr A*, as reported here.

Acknowledgments: This work is partially supported by the grant AST-0807400 from the NSF and DP0986386 from the Australian Research Council. Ongoing CARMA development and operations are supported by the National Science Foundation under a cooperative agreement, and by the CARMA partner universities.

REFERENCES

Becker, P., Das, S. & Le, T. 2011, ApJ, 743, 47

- Baganoff, F. K., et al. 2003, ApJ, 591, 891
- Cuadra, J., Nayakshin, S. & Martins, F. MNRAS, 383, 458
- Das, S., Becker, P. & Le, T. 2009, ApJ, 702, 649
- Eckart, A. et al. 1990, Nature, 355, 526
- Fruscione, A., et al. 2006, Proc. SPIE, 6270
- Falcke, H. & Markoff, S. 2000, A&A, 362, 113
- Ferriere, K. 2012, eprint arXiv:1201.6031
- Ghez, A. M., Salim, S., Weinberg, N. N., Lu, J. R., Do, T., et al. 2008, ApJ, 689, 1044
- Gillessen, S., et al. 2009, ApJ, 692, 1075
- Koyama, K. et al. 2009, PASJ, 61, 255
- Lacy, J. H., Achtermann, J. M., & Serabyn, E. 1991, ApJ 380, L71
- Lacy, J. H., Townes, C. H., Geballe, T. R., & Hollenbach, D. J. 1980, ApJ 241, 132
- Lutz, D., Krabbe, A. & Genzel, R. 1993, ApJ 418, 244
- Markoff, S., Bower, G. & Falcke, H. 2007, MNRAS, 379, 1519
- Muno, M. P., Baganoff, F.K., Brandt, W. N., Morris, M. R. and Starck, J.-L. 2008, 673, 251
- Muzic, K, Eckart, A., Schodel, R., Meyer, M. L. & Zensus, A. 2007, A&A, 469, 993
- Paumard, T. et al. 2006, ApJ, 643, 1011
- Reid, M. J. and Brunthaler, A. 2004, ApJ, 616, 872
- Roberts, D. A., & Goss, W. M. 1993, ApJS, 86, 133
- Sunyaev, R.A. & Churazov, E. 1998, MNRAS, 297, 1279
- Wang, Q. D., Lu, F. J. & Gothelf, E. V. 2006, MNRAS 367, 937
- Wardle, M., & Yusef-Zadeh, F. 308, 1992, Nature, 357, 308
- Yusef-Zadeh, F., Morris, M. & Eckers, R. D. 1990, Nature, 348, 45
- Zhao, J. H., Morris, M. R., W. M. Goss, W. M. & An, T. 2009, ApJ 699, 186

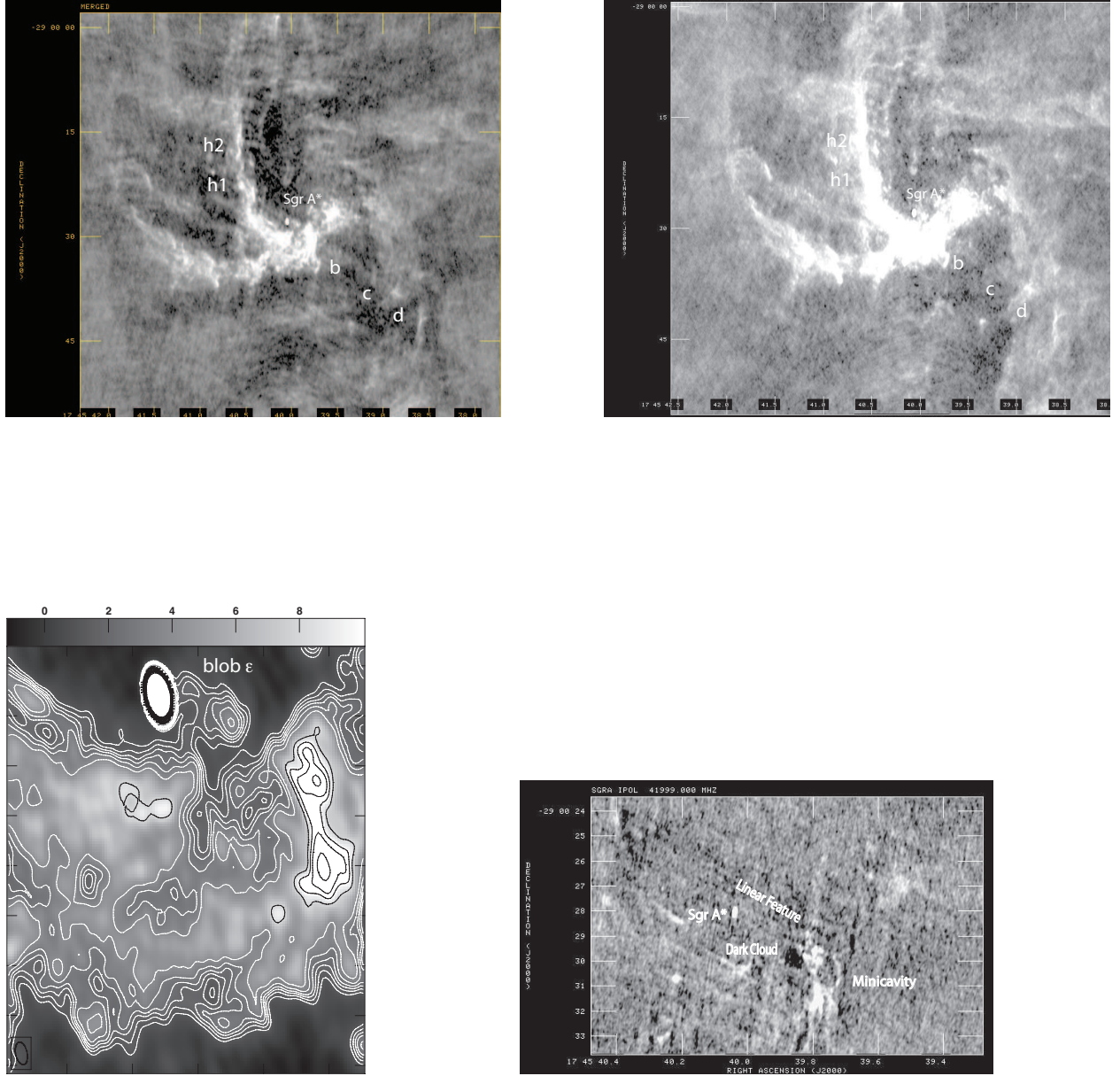


Fig. 1.— (a-b) Top 22 (left) and 15 (right) GHz VLA images constructed by combining A and B array data with resolutions of $0.36'' \times 0.18''$ (PA= 2°) and $0.36'' \times 0.20''$ (PA= -0.6°), and rms noises of 1.5×10^{-4} and 9×10^{-5} mJy beam⁻¹, respectively. (c) Bottom Left Contours of emission with a resolution of $0.46'' \times 0.23''$ (PA= -12°) at 8.4 GHz -1.2, 1.2, 1.6, 2, 2.4, 3, 4, 6, 8, 10, 12, 16, 20,..., 40 and 50 mJy beam⁻¹. (d) Bottom Right A 42 GHz image with a resolution $0.16'' \times 0.08''$ (PA= -0°).

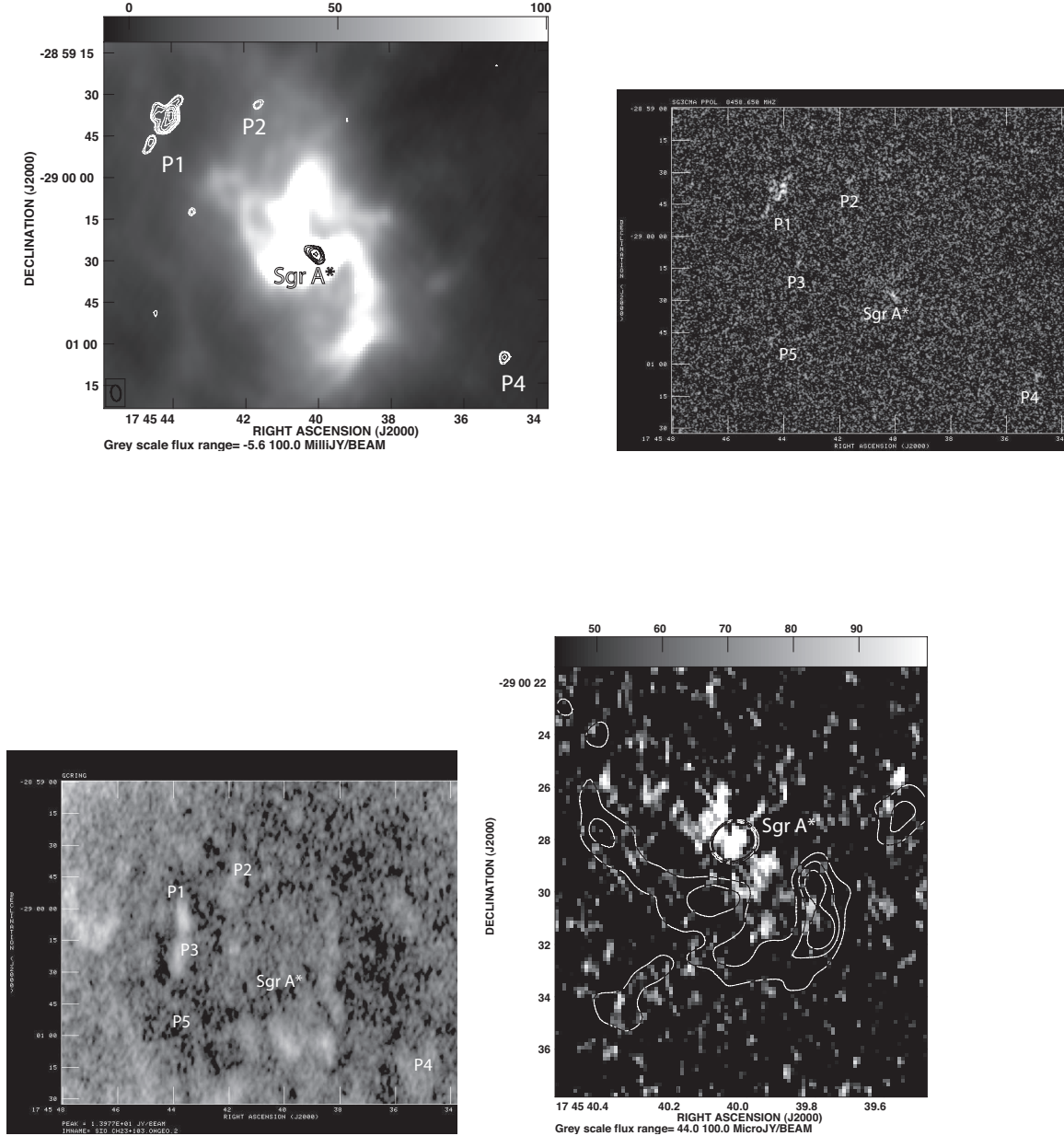


Fig. 2.— (a) Contours of 8.4 GHz polarized emission with a resolution of $10'' \times 10''$ with levels set at $(3.5, 4, 5, 6, 8, 10, 12) \times 50 \mu\text{Jy beam}^{-1}$ on a grayscale intensity image with a resolution of $5.8'' \times 3.5''$ ($PA = 7^\circ$). (b) A grayscale 8.4 GHz polarized intensity at 8.4 GHz with a resolution of $0.93'' \times 0.51''$ ($PA = -7^\circ$). (c) A grayscale distribution of SiO(2-1) emission from the CMR integrated between velocities -121.6 and 148 km s⁻¹. (d) Contours of 8.4 GHz intensity of the minicavity with levels set at 20, 30 and 40 mJy beam⁻¹ superimposed on polarized intensity from Sgr A* and its immediate vicinity. The resolution is the same as (b).

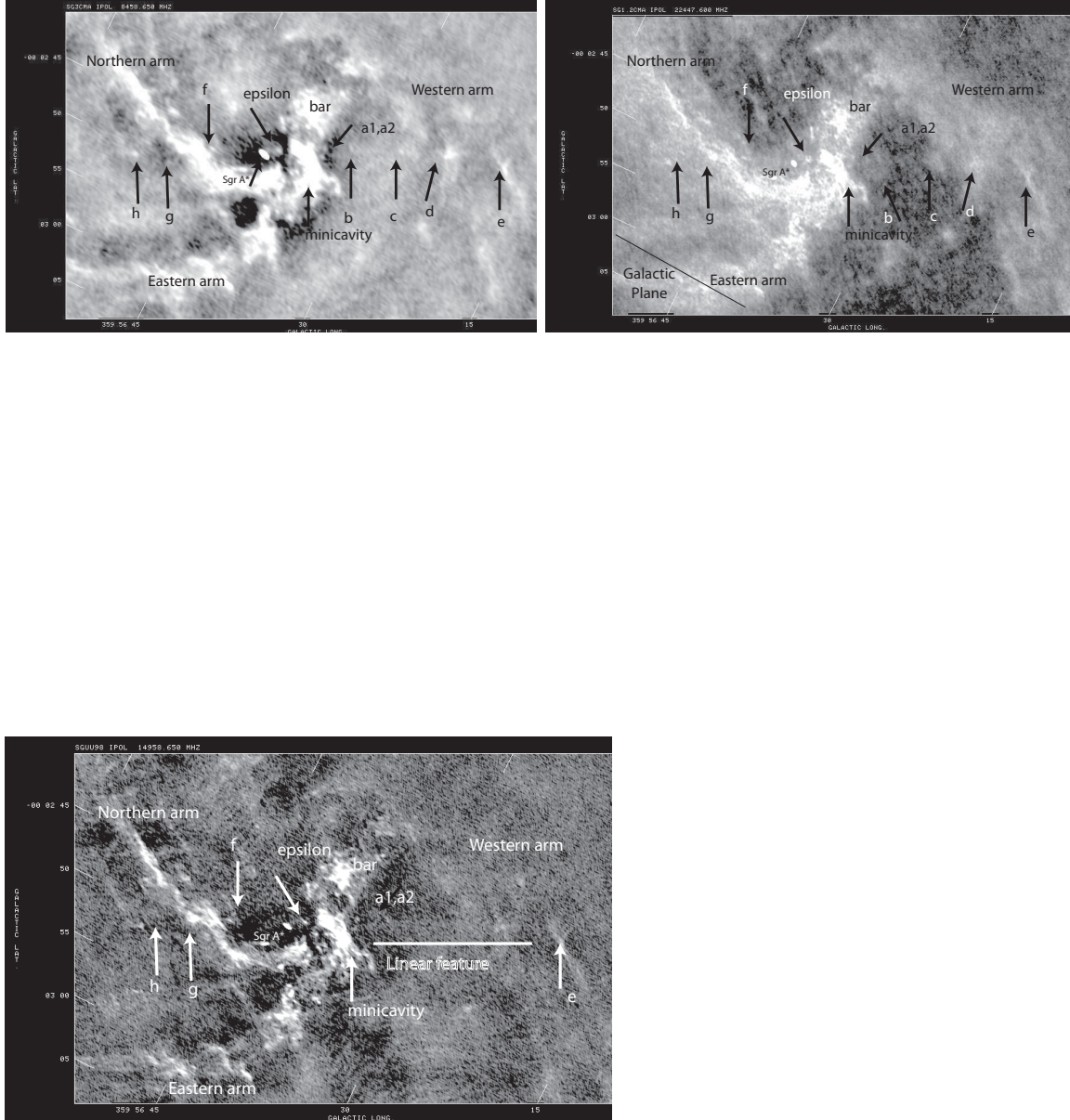


Fig. 3.— All images are rotated by $\sim 28^\circ$ with respect to the Galactic plane in order to place the linear feature along the horizontal axis. (a) A grayscale total intensity image of the inner $30'' \times 45''$ of Sgr A* at 8.4 GHz based on combining A-array configuration data sets taken on 1991-08-15 and 1990-05-30. The spatial resolution is $0.46'' \times 0.23''$ (PA= 12°). (b) Similar to (a) except at 23 GHz based on combining A, C and B-array data taken on 1990-05-30, 1986-12-28 and 1987-11-27, respectively. The resolution of the image is $0.24'' \times 0.17''$ (PA= 1.58°). (c) Similar to (a) except at 15 GHz based on A-array data taken on 1998-04-30. The resolution is $0.2'' \times 0.1''$ (PA= -0.23°).

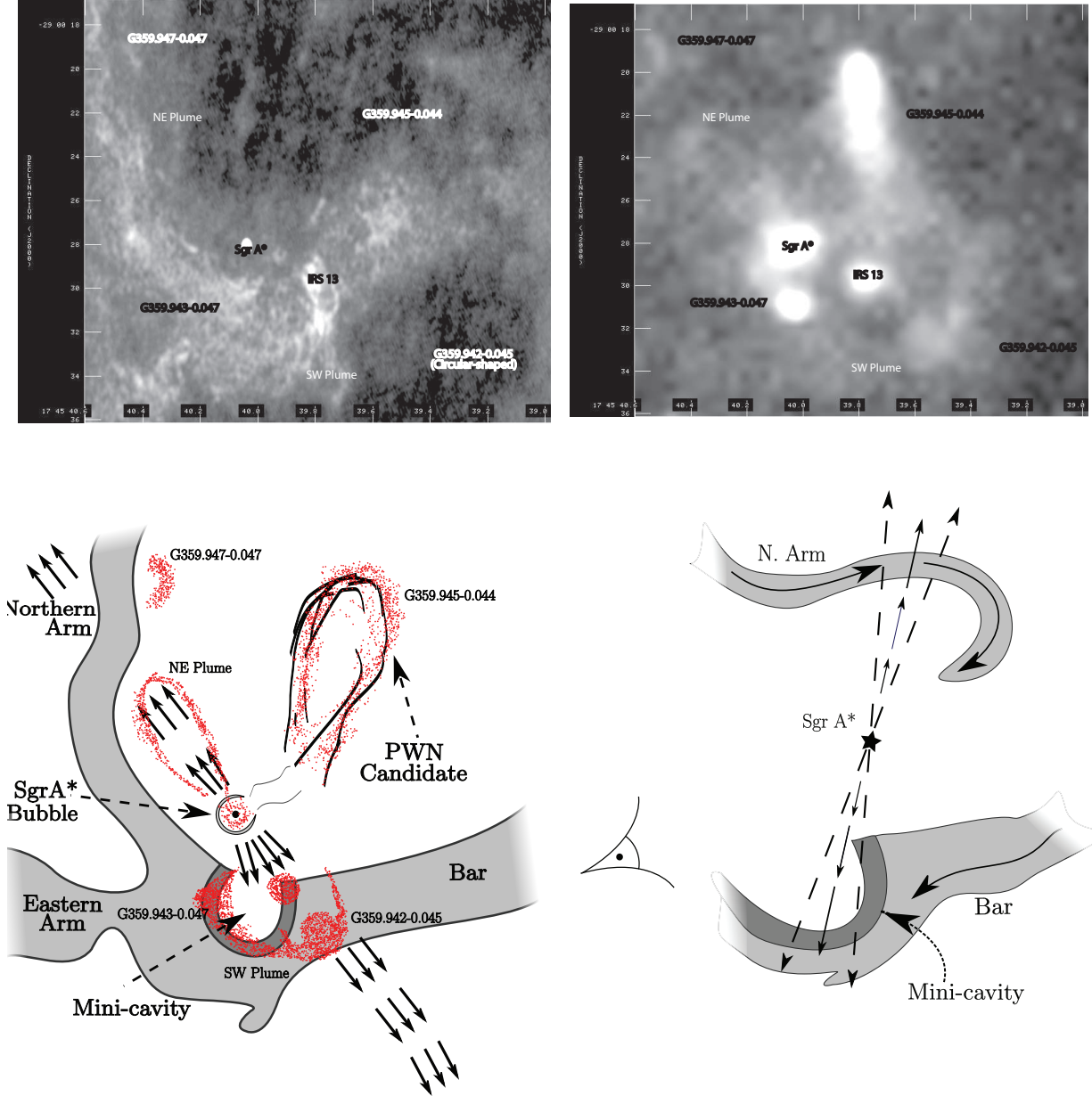


Fig. 4.— (a) A radio continuum image of Sgr A* at 22.3 GHz with a spatial resolution of $\sim 0.24'' \times 0.17''$ (PA= 1.6°). The data are taken in the A-array configuration on 1990-05-30, 1987-11-27, combined with the C-array configuration on 1986-12-28. (b) The same region as (a) but showing X-ray emission between 0.5-10keV at a resolution of $0.49''$. (c) A schematic diagram showing bright radio and X-ray features in gray and red, respectively, and a model of a narrow two-sided jet from Sgr A*. (d) A schematic diagram of a model showing the near and far side components of the symmetrical jet running into the ionized bar and the N arm which are assumed to be located in the front and back side of Sgr A*, respectively.